UCLA
UCLA Electronic Theses and Dissertations

Title
Human Perivascular Stem Cell-based Bone Graft Substitute Induces Rat Spinal Fusion

Permalink
https://escholarship.org/uc/item/77p547p6

Author
Chung, Choon Greg

Publication Date
2014

Peer reviewed|Thesis/dissertation

eScholarship.org Powered by the California Digital Library
University of California

UNIVERSITY OF CALIFORNIA

Los Angeles

Human Perivascular Stem Cell-based Bone Graft Substitute Induces Rat Spinal Fusion

A thesis submitted in partial satisfaction

of the requirements for the degree

Master of Science in Oral Biology

By

Choon Chung

2014

© Copyright by
Choon Chung
2014

ABSTRACT OF THESIS

Human Perivascular Stem Cell-based Bone Graft Substitute Induces Rat Spinal Fusion

By

Choon Chung

Master of Science in Oral Biology

University of California, Los Angeles, 2014

Professor Kang Ting, Chair

Background: Adipose tissue is an attractive source of mesenchymal stem cells (MSC) due to its abundance and accessibility. Previous studies have defined a population of native MSC termed perivascular stem cells (PSC), purified from diverse human tissues, including adipose tissue. Human (h)PSC are a homologous population composed of pericytes (CD146+CD34−CD45−) and adventitial cells (CD146−CD34+CD45−), isolated by fluorescence-activated cell sorting (FACS), with properties identical to those of culture identified MSC. The evidence supporting the use of human perivascular stem cells (hPSC) for bone tissue engineering is based on our prior studies: firstly, pancreas- (and other organ-) derived human pericytes exhibit robust *in vitro* osteogenic differentiation and intramuscular bone formation

and angiogenesis[31]; next, adipose-derived hPSC form significantly increased intramuscular bone compared to patient-matched unpurified cells and demonstrate *in vivo* trophic and angiogenic effects[32,33], and lastly adipose-derived hPSC exhibited improved calvarial bone defect healing as compared to unsorted SVF[34].

Methods: Athymic rats(n=5-6 per treatment group) were randomly distributed into four treatment groups of escalating human PSC(hPSC) dose, delivered on a demineralized bone matrix scaffold. After four weeks, animals were sacrificed and spinal fusion was assessed by manual palpation, high-resolution micro-Computed Tomography(microCT) and histology. Computerized biomechanical assays were performed using finite element analysis(FEA). Finally, immunohistochemistry, with anti-human/anti-rat Major Histocompatibility Complex Class (MHC) Class I, was performed to assay the origin of newly formed bone.

Results: Treatment with hPSC successfully induced 80-100% fusion by four weeks compared to acellular-treated controls (20% fusion), confirmed by microCT and histological analyses. Biomechanically, it was observed that hPSC treatment induced more sound bone, capable of withstanding significantly higher force compared to control. Lastly, using immunostaining, it was observed that rat-specific osteoblasts outnumbered human-specific osteoblasts by a ratio of 3.9-10:1. Likewise, rat-specific osteocytes outnumbered human-specific osteocytes by a ratio of 7.8-30.8:1, indicating that hPSC operate to a large degree via paracrine signaling. Immunohistochemistry for species-specific antigens verified that hPSC play a direct role in bone formation, but also that hPSC play a role in paracrine support of host osteoprogenitor cell recruitment and/or differentiation.

Conclusion: hPSC are a readily available MSC population that effectively forms bone without requirements for culture, pre-differentiation or exogenous cytokine stimulation. Thus, hPSC-based products show promise for future efforts in clinical bone regeneration and repair.

The thesis of Choon Chung is approved.

_____
Kang Ting, Committee Chair

_____
Xinli Zhang

_____
Soritos Tetradis

_____
Yong Kim

University of California, Los Angeles

2014

This thesis is dedicated to

Dr. Ting, Dr. Soo, and Dr. Zhang for all their academic guidance

and my family especially my wife and son

who have supported me throughout my life.

TABLE OF CONTENTS

List of Figures vii

Introduction 1

Materials and Methods 9

Results 14

Discussion 30

References 33

LIST OF FIGURES

Figure 1 Manual palpation ……...15

Figure 2 Micro-Computed Tomography (microCT) Analysis ……17

Figure 3 Biomechanical / Finite Element Analysis……...……...18

Figure 4 Histological Analyses….....20

Figure 5 Species-Specific MHC Analyses.....22

Figure 6 Bone Labeling Analyses.....23

Acknowledgements

This work was supported by the CIRM Early Translational II Research Award TR2-01821, NIH/NIDCR (grants R21 DE0177711 and RO1 DE01607), and UC Discovery Grant 07-10677.

K.T., B.P., and C.S. are inventors of perivascular stem cell-related patents filed from UCLA. Drs. K.T, and C.S. are founders of Scarless Laboratories Inc. which sublicenses perivascular stem cell-related patents from the UC Regents, and who also hold equity in the company. Dr. Chia Soo is also an officer of Scarless Laboratories, Inc.

Human Perivascular Stem Cell-based Bone Graft Substitute Induces Rat Spinal Fusion

INTRODUCTION

Skeletal diseases, whether congenital or acquired, are one of the most frequent and costly medical conditions, and are expected to increase as the US population continues to age. The escalating burden of musculoskeletal diseases is depicted through its rising cost in the US; in 1992, the total cost of musculoskeletal diseases incurred $149.4 billion, while in 2004, the cost has risen to $849 billion, equivalent to 7.7% of the (GDP)[1,2]. Specifically, spinal fusion procedures have become ubiquitous, with over 350,000 spinal fusions performed per annum in the United States; a 200% increase over the past decade [3-7]. Currently, autogenous bone grafting is considered the gold standard for skeletal reconstruction. However, limited availability and significant complications (such as donor site morbidity, increased operative and recovery time, and pain) have prompted the search for safer and more effective alternatives[8-10]. Mesenchymal stem cells (MSC) are multipotent stromal cells capable of regenerating mesenchymal tissues. Well studied for their application in skeletal engineering, bone marrow mesenchymal stem cells (BMSC) are the main source of MSC for bone regeneration[11-13]. However, distinct disadvantages exist for the use of BMSC, such as limited autogenous supply, requirement for culture based derivation and expansion, and reduced cellular activity in aged or osteoporotic patients[14,15].

Another promising source of MSC is adipose tissue, as this source is highly

accessible and abundant. Adipose derived stem cells demonstrate clear advantages over BMSC in availability; yet, *in vitro* cell culture increases the risk of immunogenicity, genetic instability, and infection[16-21]. To circumvent these risks, interest has risen in the use of the non-cultured stromal vascular fraction (SVF) of adipose tissue among such companies as IntelliCell™ and Cytori Therapeutics, Inc. However, SVF is well recognized to be a heterogenous population including non-stem cells, such as inflammatory, hematopoietic, and endothelial cells, which results in unreliable bone formation[22-24]. With these drawbacks of currently available MSC sources, there exists a clinical need for a reliable source of MSC with proven safety, purity, identity, and efficacy.

Our laboratory has identified and isolated perivascular stem cells (PSC) from multiple vascularized tissues using a fluorescence-activated cell sorting (FACS) method[25-29]. PSC are identified by their cell surface markers and include pericytes from microvessels and capillaries (which are CD34-, CD146+, CD45-) (**Fig. 1**) ,

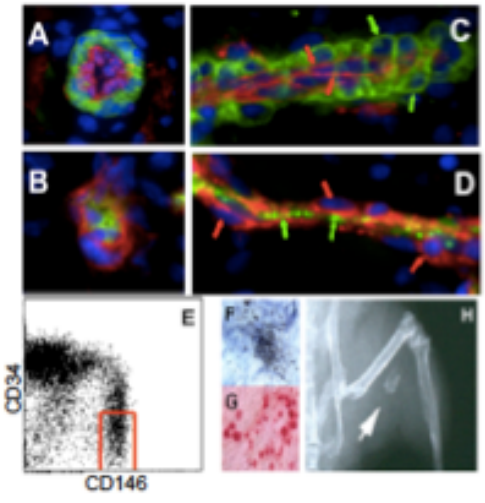

Figure 1. Pericytic MSC. All human pericytes express CD146 (A, green; endothelial CD34 is red; B, red; CD34 is green), NG2 (C, green; endothelial VE-cadherin is red) and PDGF-Rβ (D, red; endothelial von Willebrand factor (vWF) is green). E: Pericytes are purified by FACS as CD45-CD56-CD146+CD34- cells (red gate). Pericytes cultivated in osteogenic medium for 21 days: F, von Kossa staining; mineral deposits appear in black. G, alizarin red staining; calcium deposits are stained red. H: Pericytes embedded in a Gelfoam sponge in the presence of BMP2 were implanted in a SCID-NOD mouse muscle pocket. X-ray analysis at day 30 after implantation.

and adventitial cells from larger arteries and veins (which are CD34+, CD146-, CD45-) (**Fig. 2**) [30].

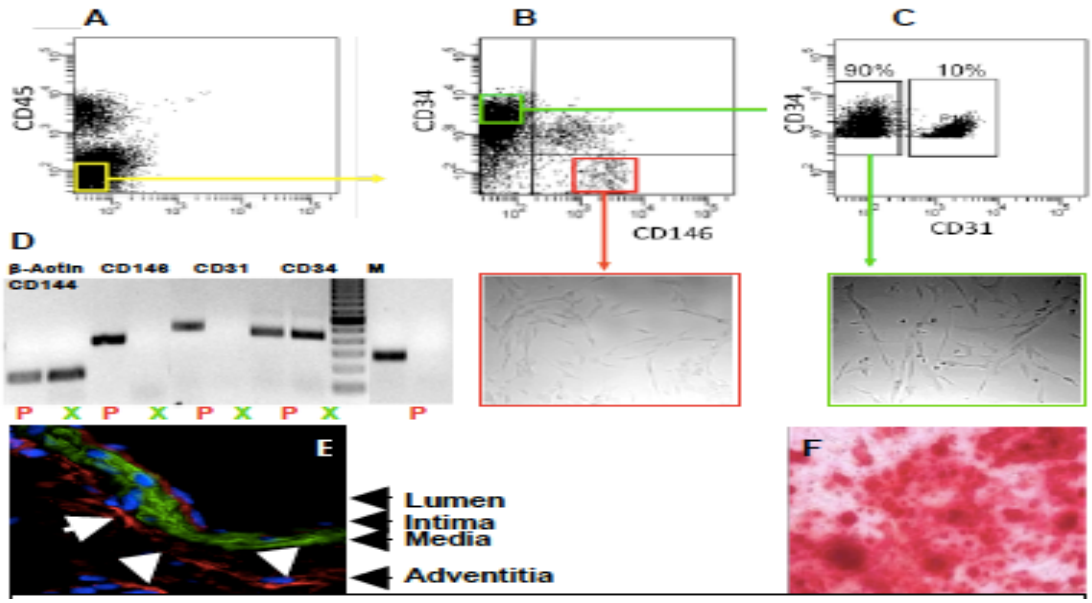

Adventitial cells. (A,B) Pericytes were sorted from adipose tissue (red), as well as CD146-CD34hi cells (green), also endowed with MSC potential. (C) CD146-CD34high cells were further divided into CD31+ and CD31- cells, only the latter gave rise to MSC. Sorted CD146-CD34high CD31-cells (x) are not contaminated by endothelial cells or pericytes (D). (E) CD146-CD34hi CD31- cells (arrows) are all localized in the tunica adventitia of larger blood vessels (CD34 in red). (F) Purified adventitial MSC are osteogenic in vitro (alizarin red staining).

PSC exhibit the characteristic surface markers and clonal multilineage differentiation potential of MSC[25-29]. The evidence supporting the use of human perivascular stem

cells (hPSC) for bone tissue engineering is based on our prior studies: firstly, pancreas- (and other organ-) derived human pericytes exhibit robust *in vitro* osteogenic differentiation and intramuscular bone formation and angiogenesis[31]; next, adipose-derived hPSC form significantly increased intramuscular bone compared to patient-matched unpurified cells and demonstrate *in vivo* trophic and angiogenic effects[32,33] (**Fig. 3**) ,

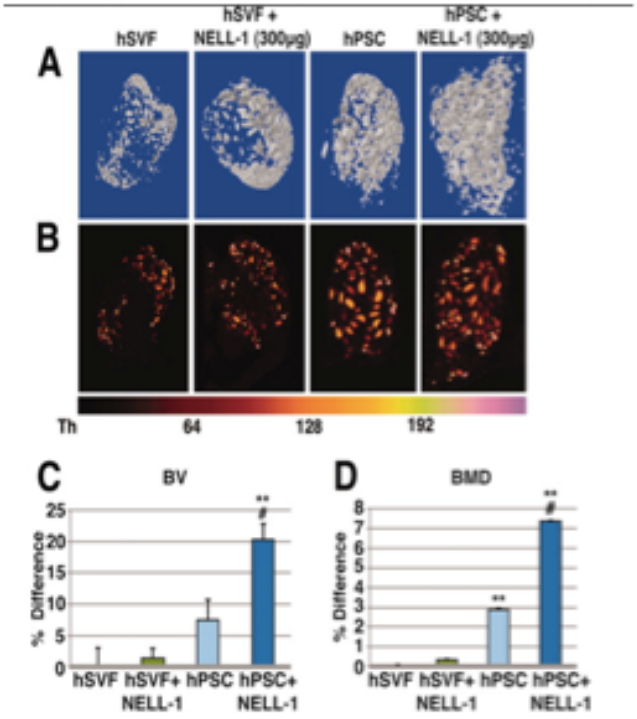

Figure 3. Effects of NELL-1 on hPSC- or hSVF-mediated ectopic bone formation. hSVF or hPSCs in a SCID mouse muscle pouch with DBX Putty, with or without NELL-1, assessed at 4 weeks postimplantation. See supplemental online Table 6 for treatment groups. (A): Representative three-dimensional microcomputed tomography (microCT) reconstructions. Threshold (Th) 90 was used. (B): Colorized representative two-dimensional microCT images. A scale bar below indicates colorization at various thresholds. (C): Relative BV; Th50–120 used. (D): Relative BMD

and lastly adipose-derived hPSC exhibited improved calvarial bone defect healing as compared to unsorted SVF[34] (**Fig. 4**).

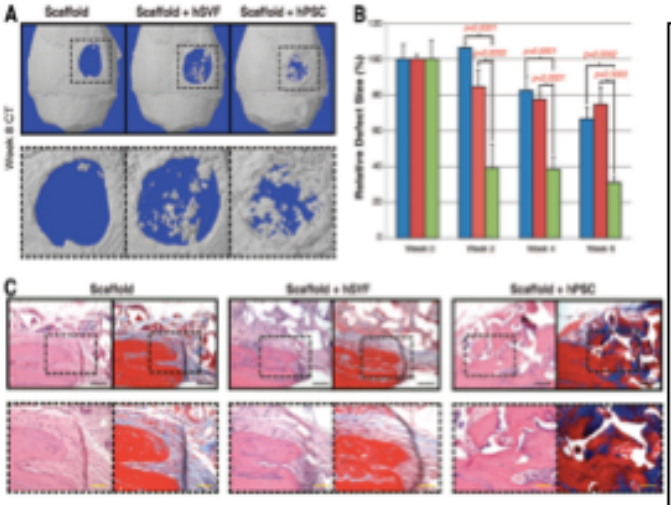

Figure 4. Calvarial healing by microCT and histology. hSVF or hPSCs were used to treat a 3-mm-diameter parietal bone defect in a SCID mouse. **(A):** Three-dimensional reconstructions of control, hSVF-treated, or hPSC-treated calvarial defects shown at 8 weeks postoperative.**(B):** Relative defect healing as assessed by 0, 2, 4, and 6 weeks postoperative by serial live microCT scans. **(C):** Representative H&E and Masson's trichrome images for the defect site.

In the present study, we sought to translate the regenerative potential of hPSC to a functionally demanding rat spinal fusion model. We observed that hPSC treatment induces endochondral bone formation and rigid mechanical fixation of the lumbar spine in rats, as compared to an acellular control.

MATERIALS AND METHODS

Isolation of hSVF from human lipoaspirate and purification of hPSC from hSVF

Human lipoaspirate was collected from cosmetic liposuction patients (n=4 patients). The whole lipoaspirate was stored at 4°C before processing and processed within 48 h of collection. The human stromal vascular fraction (hSVF) was obtained by collagenase digestion as previously described[30]. Briefly, an equal volume of phosphate buffered saline (PBS) was added to dilute the lipoaspirate. The mixture was then digested with Dulbecco's modified Eagle's medium containing 3.5% bovine serum albumin (BSA, Sigma-Aldrich) and 1mg/ml collagenase type II for 70 min under agitation at 37°C. Next, adipocytes were separated and excluded by centrifugation. The processed hSVF was suspended in red cell lysis buffer (155 mM NH_4Cl, 10 mM $KHCO_3$, and 0.1mM EDTA) and incubated for 10 min at room temperature. The incubated hSVF was re-suspended in PBS and 4', 6-diamidino-2-phenylindole (DAPI, Invitrogen) was added to exclude dead cells and filtered through a 70 μm cell filter. The resulting hSVF was immediately processed for hPSC purification. The number of live cells was calculated by trypan blue staining. Patient demographics for the lipoaspirate used, including gender, age, and anatomic location is presented in (**Table 1**).

Table 1:

Gender	Age (years)	Anatomical location(s)	BMI (kg/m²)
Male	60	C	23.7
Female	41	Fl, H, T	22.5
Female	40	Abd, Fl, H	29.2
Female	37	Abd, A, B, H, Fl	28.3

[1]Demographic of lipoaspirates. Acronyms: A: Arms; Abd: Abdomen; B: Back; BMI: Body Mass Index; C: Chest; Fl: Flank; H: Hip; T: Thigh.

Purification of hPSC from hSVF

hPSC were purified from the isolated hSVF by FACS as previously described[30,34]. Briefly, hSVF was incubated at 4°C for 15 min in dark surroundings with the following conjugated antibodies: anti-CD34-phycoerythrin (Dako), anti-CD45-allophycocyanin (Santa Cruz Biotechnology, Inc.), and anti-CD146- fluorescein isothiocyanate (AbD Serotec). Next, DAPI was added to remove any nonviable cells from the mixture. The resulting cell population was processed on the FACS Aria cell sorter (BD Biosciences). Consequently, two populations of cells were sorted according to their cell surface markers to constitute hPSC, distinct pericytes (CD34-, CD146+, CD45-), and adventitial cells (CD34+, CD146-, CD45-)[25,28,29].

Implant preparation

Demineralized bone matrix (DBX) putty (300 ul per side; ovine source, Musculoskeletal Transplant Foundation), a combination of morselized cortical and cancellous bone chips mixed with sodium hyaluronate, was used as a scaffold for cell delivery. Defined numbers of cells were suspended in 50 µl of PBS and mixed mechanically with DBX particles. Cell numbers and concentrations were based on previously published data[32] and are fully described in (**Table 2**). Implants were kept on ice prior to *in vivo* implantation.

Table 2:

Treatment Group[1]	Sample size (N)	Concentration
Control	5	0 cells/mL
0.15 x 10^6 hPSC	6	0.25 x 10^6 cells/mL
0.50 x 10^6 hPSC	5	0.83 x 10^6 cells/mL
1.50 x 10^6 hPSC	6	2.50 x 10^6 cells/mL

[1]Treatment groups for study. Note that 300 ul of demineralized bone matrix scaffold was implanted per side. Acronyms: DBX: Demineralized bone matrix; hPSC: human perivascular stem cell; N: number.

Animal model and surgical procedures

Athymic rats were used to prevent immune response to human cells. All animals were treated with postoperative medications of buprenorphine for 48 h and

trimethiprim/sulfamethoxazole for 10 days, for pain management and prevention of infection, respectively. Animals were housed and experiments were performed in accordance with the guidelines of the Chancellor's Animal Research Committee for Protection of Research Subjects at the University of California, Los Angeles.

Posterolateral lumbar spinal fusion was performed on n= 23, 8 week old athymic rats as previously described [35]. Rats were anesthetized using isoflurane (5% induction, 2-3% maintenance). Posterior midline incisions were made over the caudal portion of the lumbar spine and two separate fascial incisions were made 4 mm bilaterally from the midline. Blunt muscle splitting technique was used lateral to the facet joints to expose the transverse processes of L4 and L5 lumbar spines. The processes were then decorticated using a low speed burr under regular irrigation with sterile saline solution to cool the decortication site and maintain a clean surface for implantation. Next, the treatment material was delivered via a scaffold, implanted between the transverse processes bilaterally into the paraspinal muscle bed. Finally, the fasciae and skin were each closed using a simple continuous technique with 4-0 vicryl sutures (Ethicon). Rats were sacrificed four weeks post-surgery via CO_2 overdose and the spines were harvested for analysis.

Manual palpation

At 4 weeks post implantation, the lumbar spine specimens were retrieved *en bloc*. Manual palpation was performed to evaluate the reduction of motion between the lumbar

spines of rats post harvest. The samples were palpated by three blinded observers and scored on a scale of 1 to 5 by application of flexion and extension forces manually against the L4 and L5 vertebrae as previously described[36]. The scoring criteria were as follows; 1, motion between vertebrae, with no bone mass formation; 2, motion with a unilateral bony mass; 3, motion with bilateral bony masses; 4, no motion between vertebrae, with moderate bilateral bone masses bridging transverse processes; 5, no motion, with abundant bilateral bone masses bridging transverse processes. Scores of four or above were considered as reflective of spinal fusion.

High-resolution quantitative micro-CT analysis

In preparation for micro-CT imaging, all samples were stored in 4% paraformaldehyde for 48 hours. Samples were scanned using high-resolution micro-CT (Skyscan 1172F, Skyscan) at an image resolution of 20 μm (55 kV and 181 mA radiation source, using a 0.5 mm aluminum filter) and analyzed using DataViewer, Recon, CTAn, and CTVol software provided by the manufacturer. All quantitative and structural parameters follow the nomenclatures described by the American Society for Bone and Mineral Research Nomenclature Committee[37].

3D data analysis was carried out by manually drawing polygonal regions of interest (ROIs) designed to encircle the newly formed bone mass between the L4 and L5 transverse processes. Regions of interest were designed to include the implant material and newly formed bone, but exclude pre-existing bone structures. Analyses included

bone mineral density, bone volume / tissue volume (bone volume density), trabecular thickness (Tb. Th), trabecular spacing (Tb. Sp), and trabecular number (Tb. N). A threshold value range of 60 - 120 was selected to best represent the newly formed bone using a global thresholding technique[37].

Biomechanical analysis (Finite element analysis)

To determine three-dimensional quantities, such as the subtle changes in microstructural and mechanical properties of bone, we chose to use computerized biomechanical simulation. Direct experimental assessments are plagued with large errors and uncertain significance[38-40]. Therefore, to more accurately evaluate the biomechanical properties of fusion in the bilateral bone bridge, we used finite element models to simulate real mechanical tests. In order to accomplish this, micro-CT images were converted to DICOM files using SkyScan Dicom Converter software (DicomCT application, Skyscan 1172F, Skyscan). Macro and micro simulations were performed to evaluate the biomechanical properties of the fusion sites. First, tetrahedral three-dimensional mesh models were created by drawing a ROI to isolate L4 and L5 lumbar vertebrae and their respective newly formed fusion masses, using ScanIP software (Simpleware Limited). Secondly, tetrahedral 3D cube shaped mesh models with a dimension of 2mm × 2mm × 2mm were created from both the right and left sides of newly formed bone of the fusion site through a threshold segmentation process set at 1250-4095 gray levels using Mimics software (version 16.0; Materialise, Leuven, Belgium). 3-matic (version 8.0; Materialise, Leuven, Belgium) was used to remesh these 3D mesh models with a shape quality

threshold of 0.3 Height/Area, and a maximum triangle edge length of 0.1 mm. Following remeshing, the 3D cube models had an average of 110,000 elements. Finite element analyses were performed using the ABAQUS software (version 6.12; Dassault Systèmes, Velizy-Villacoublay, France). Material properties of cancellous bone were considered to be isotropic, homogenous, and linearly elastic with an elastic modulus of 3.5 GPa and a Poisson's Ratio of 0.25[41]. Boundary conditions constrained all displacements and rotations on the lower (caudal) border nodes of the L5 vertebral body and 3D cube models. Next, we applied a uniform compressive stress force of 0.5 MPa on the superior surface of the L4 vertebral body and 3D cube models, to reproduce human intradiscal pressure experienced in relaxed standing to the upper (rostral) border nodes of the L4 vertebral body[42]. Finally, the mean von Mises stress experienced of the samples were analyzed.

Histology and immunohistochemistry analysis

After micro-CT analysis, samples were decalcified using 19% ethylenediaminetetraacetic acid (EDTA) and embedded in paraffin. Hematoxylin and eosin (H&E) and Masson's trichrome staining were performed on deparaffinized sections following standard protocols [31]. Next, immunohistochemical staining was performed with primary antibodies against both human and rat major histocompatibility complex (MHC) Class I antigens (Santa Cruz Biotechnology), Osteocalcin (OCN) (Santa Cruz Biotechnology), and Bone Sialoprotein (BSP) (Chemicon) using the ABC (Vector Laboratories, Inc.) method. Immunohistochemistry was performed after paraffin slices were deparaffinized,

dehydrated, rinsed, and incubated with 3% H_2O_2 for 20 min. All sections were then blocked with 0.1% bovine serum albumin in PBS for 1 h. At a dilution of 1:100, primary antibodies were added to each section and incubated at 37°C for 1 h or overnight at 4°C. Images were obtained on an Olympus BX51 fluorescence microscope. For selected experiments, bone formation was quantified by blinded histomorphometric analyses using H&E staining and Photoshop (Adobe Systems Inc) quantification as expressed by bone area/total implant tissue area. Additionally, selected immunohistochemistry samples had semi-quantifications of positive staining performed using the magic wand tool in Adobe Photoshop with a tolerance setting of 30. Semi-quantification of positive staining in OCN and BSP stained samples was also performed. Finally, to investigate the origin of the differentiated osteoblasts and osteocytes, species specific quantification of positive staining of MHC was performed. .

Bone labeling and histomorphometric analysis

To visualize the bone forming activity of each treatment group, animals from each groups were divided into two different *in vivo* labeling groups for bone histomorphometric analysis; 1) calcein-calcein intraperitoneal injections and 2) calcein-demeclocycline intraperitoneal injections. Animals were injected with calcein (20 mg/kg) nine days prior to sacrifice and followed by either an identical dose of calcein or demeclocycline (6 mg/kg) two days before sacrifice. The time interval between the two injections was one week. Images were obtained using an Olympus BX51 fluorescence microscope. To compensate for the irregularity of DBX scaffold implants, instead of measuring the

length between the two intervals, semi-quantification was performed as a relative percent positive fluorescence over control value.

Statistical analysis

Statistical analysis was performed using the appropriate analysis of variance (ANOVA) to analyze more than two groups, followed by post hoc Tukey's test analysis between specific groups. $*p < 0.05$ and $**p < 0.01$ were considered to be significant.

RESULTS

Evaluation of Spinal Fusion using Manual Palpation

At four weeks post implantation, flexion/extension forces were used to evaluate gross intervertebral motion. Fusion was graded using a five-point scale, as previously described[41,43], with a score of 4 or greater considered fused. hPSC treatment resulted in significantly increased spinal fusion rates in comparison to the acellular control. All three dosages of hPSC (0.15×10^6, 0.5×10^6, and 1.5×10^6) resulted in fusion rates of 100%, 80%, and 100% respectively, compared to 20% fusion in the acellular control group (**Fig. 5**). In summary, hPSC treated spines demonstrated a high frequency of lumbar spinal fusion.

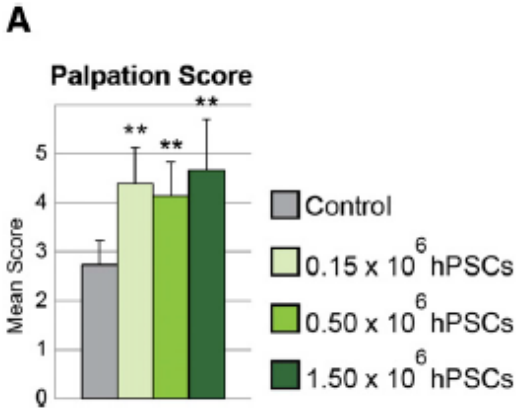

B

Treatment Group	Fusion Rate
Control	20%
0.15×10^6 hPSCs	100%**
0.50×10^6 hPSCs	80%**
1.50×10^6 hPSCs	100%**

Figure 1. Manual Palpation. Acellular control was compared to three concentrations of hPSC based bone graft substitutes. Spines were harvested four weeks post-operative, and analyzed by manually applying flexion and extension forces against the L4/L5 vertebrae. **(A)** An average score ≥4 was considered fused. **(B)** Fusion was apparent in 20% (1/5) of control-treated samples and 100% (6/6), 80% (4/5) and 100% (6/6) in 0.15×10^6, 0.50×10^6, and 1.50×10^6 hPSC-treated animals, respectively. $^{**}p \leq 0.01$ compared to control. No significant difference in fusion scores or rates was observed between hPSC-treated groups.

Evaluation of Spinal Fusion using High-Resolution Micro-CT

Having demonstrated by manual palpation that hPSC significantly enhance functional and mechanical stability, we next performed quantitative high-resolution micro-CT analyses. Three-dimensional reconstructions of the spines displayed large bilateral bone masses at level L4:L5 in hPSC-treated groups with bone bridging between adjacent transverse processes suggesting complete bony fusion (**Fig. 6A**). In contrast, the acellular control group demonstrated significantly reduced bone formation, as well as clear clefts between the two transverse processes, indicating incomplete fusion (**Fig. 6A**).

Next, micro-CT data analysis was performed to quantify the newly formed bone. hPSC-treated groups demonstrated a dose dependent trend of increased bone mineral density (BMD) (**Fig. 6B**). In hPSC-treated samples, the bone volume density (or bone volume / tissue volume (BV / TV)) exhibited a statistically significant increase as compared to the acellular control group (**Fig. 6C**). In addition, hPSC-treated groups displayed a trend toward increased trabecular thickness (Tb. Th) (**Fig. 6D**) and statistically significant dose dependent increase in the trabecular bone number (Tb. N) (**Fig. 6E**).

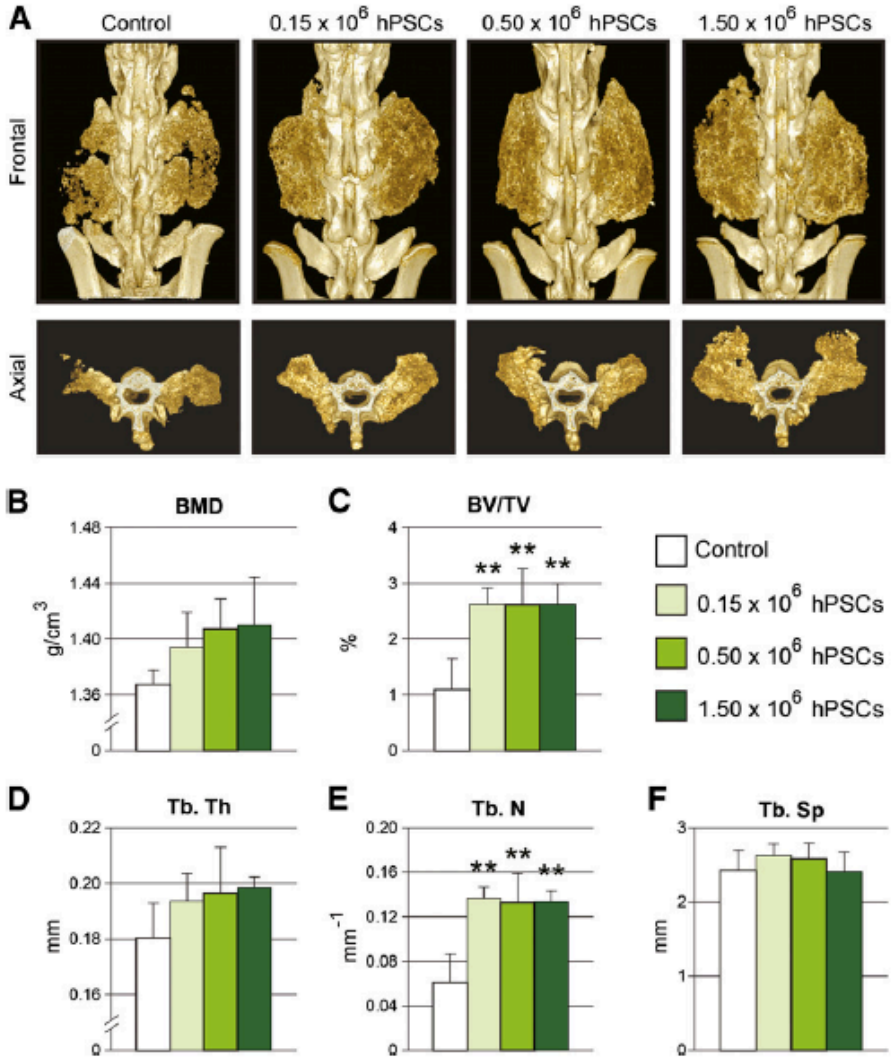

Figure 2. Micro-Computed Tomography (microCT) Analysis. (A) Reconstructions of high-resolution microCT scans, shown in frontal and axial planes. MicroCT quantifications were next performed for: (B) Bone Mineral Density (BMD), (C) Fractional Bone Volume (BV/TV), (D) Trabecular Thickness (Tb. Th), (E) Trabecular Number (Tb. N), and (F) Trabecular Spacing (Tb. Sp). $^{**}p \leq 0.01$ compared to control. No significant difference in microCT parameters was observed between hPSC-treated groups.

Evaluation of Biomechanical Properties using Finite Element Analysis

Micro-CT analyses demonstrated that hPSC treatment induced robust bone formation, however, unlike ectopic bone formation and simple bone injury models, it is essential to test the biomechanical function in a spinal fusion model. Finite element analysis (FEA) revealed that hPSC treatment resulted in bilateral bone bridging with mechanical stress distributed evenly within a range of 0 (blue) to 10 (cyan) MPa (**Fig. 7A**).

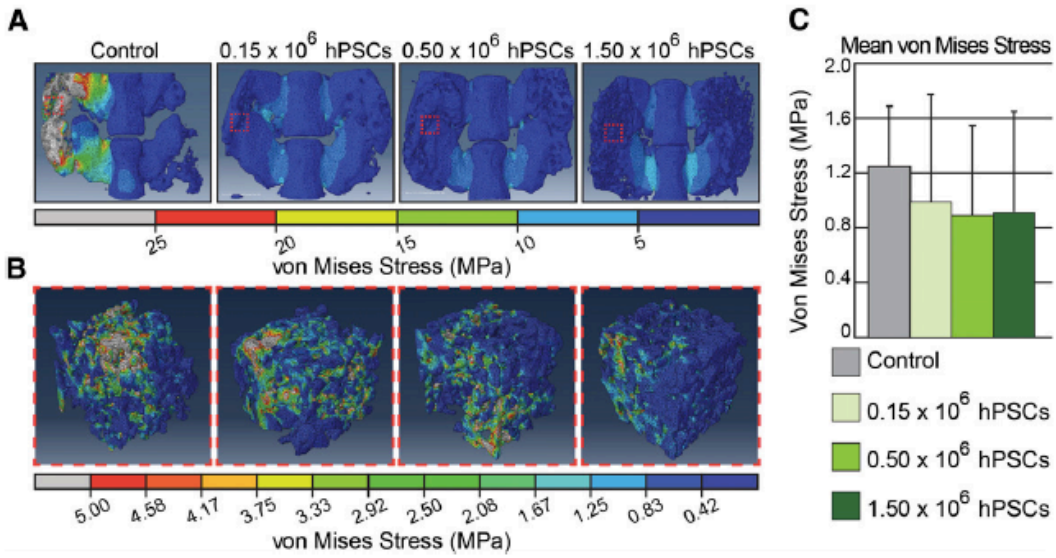

Figure 3. Biomechanical / Finite Element Analysis. (A) A uniform compressive stress force of 0.5 MPa was applied on the superior surface of the L4/L5 spinal segment. (Grey colored scale bar indicates all values exceeding 25 MPa). (B) Cuboidal specimens from newly formed bone were next assessed for von Mises stress. (C) Quantification of cuboidal segments of newly formed bone for mean von Mises stress.

Contrastingly, stress distribution was concentrated to the small areas of bony bridge formation in the acellular control group. As a result, von Mises stress values exceeded the maximum stress bearing limit of 25 (grey) MPa in the control group (**Fig. 7A**). Next, to assess bone strength within the newly formed bone, a randomly selected 2mm x 2 mm x 2mm cuboidal structure was isolated and evaluated by FEA for von Mises stress values (**Fig. 7B**). By both qualitative and qualitative parameters, all hPSC-treated groups exhibited decreased stress levels as compared to acellular control groups (**Fig. 7C**). In summary, biomechanical testing through finite element analysis further verified increased biomechanical stability and strength of spinal fusion in hPSC-implanted groups, in comparison to the acellular control group.

Evaluation of Bone Formation using Histological and Immunohistochemical Analyses

To further explore the effects of hPSC in promoting bone formation, histological analyses were performed by routine H&E and Masson's Trichrome staining (**Fig. 8A, 8B**). The acellular control group showed decellularized cortical / cancellous bone chips (DBX material) in a predominantly hypocellular fibrous background, with minimal new-formed woven bone (**Fig. 8A, 8B**). In marked contrast, hPSC-treated groups depicted DBX material connected and contiguous with significant new-formed woven bone. Moreover, with escalating hPSC dosing, an increase in hypertrophic chondrocytes was observed indicative of active endochondral ossification (**Fig. 8A**, yellow arrows). Increased osteoid was also observed in a slight dose-dependent manner in hPSC-treated samples (**Fig. 8B**, green arrows). Further, histomorphometric quantification of bone area/total implant tissue

area revealed significantly increased bone in hPSC-implanted samples as compared to the acellular control group, with a slight hPSC dose-dependent effect (**Fig. 8C**).

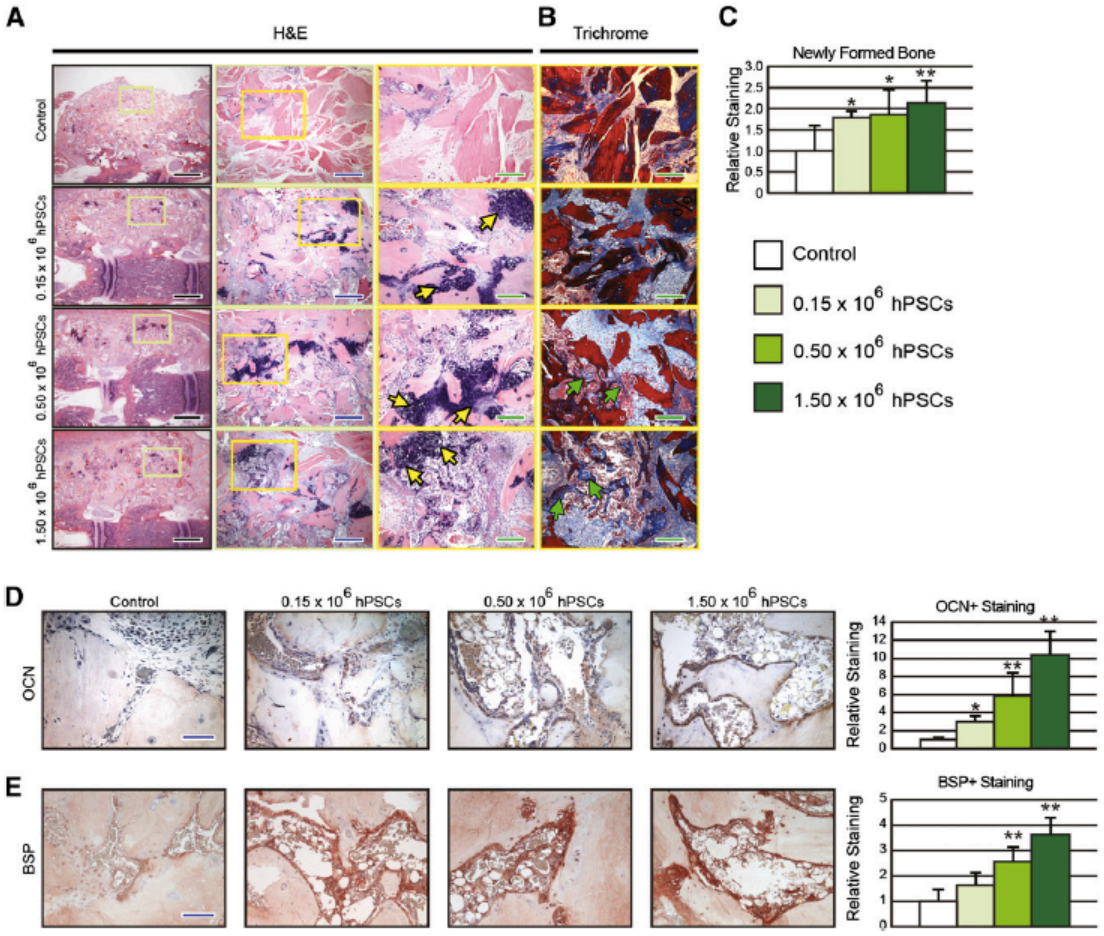

Figure 4. Histological Analyses. Coronal sections of spinal fusion stained with (A) Hematoxylin & Eosin (H&E) and (B) Masson's Trichrome. (C) Quantification for fractional Bone Area (% B.Ar). (D) Representative Osteocalcin (OCN) and (E) Bone Sialoproetin (BSP), immunohistochemical staining and quantification. yellow arrows: hypertrophic chondrocytes, green arrow: osteoid. black scale bar: 0.5cm, blue scale bar: 100μm, green scale bar: 50μm; *$p \leq 0.05$, **$p \leq 0.01$ compared to control. A slight dose-dependent effect was observed in histomorphometric analysis between hPSC-treated groups.

To confirm that hPSC-treatment induced increased endochondral bone formation, we performed immunostains for Osteocalcin (OCN), a late marker of osteogenesis. We observed that hPSC-treated samples exhibited both a significant and dose-dependent increase in OCN staining compared to acellular control (**Fig. 8D**). Additionally, we examined the efficiency of hPSC in promoting osteoblast and bone formation through Bone Sialoprotein (BSP) positive staining. Once again, hPSC-treated groups showed significantly increased relative staining in a dose dependent manner **(Fig. 8E)**.

Immunohistochemical staining for human-specific (h)MHC confirmed that with increasing doses of hPSC application, increasing human antigen staining was observed (**Fig. 9A**). This was quantified as the number of hMHC positive bone-lining osteoblasts and bone-resident osteocytes (**Fig. 9C,D**). These results showed that hPSC have a direct effect in new bone formation. Next, parallel staining was performed using rat-specific (r)MHC (**Fig. 9B**). Similar to the pattern of hMHC expression, with increasing dosages of hPSC an increasing amount of rat-specific MHC staining was observed. When quantified, an increase in both rMHC positive, cuboidal, bone-lining osteoblasts and bone-resident osteocytes was observed with increasing dosages of hPSC (**Fig. 9C,D**). Notably, rat-specific osteoblasts outnumbered human-specific osteoblasts by a ratio of 3.9-10:1 (**Fig. 9C**). Likewise, rat-specific osteocytes outnumbered human-specific osteocytes by a ratio of 7.8-30.8:1 (**Fig. 9D**). Interestingly, a significant number of human-derived osteoblast and osteocytes persisted indicating direct differentiation and incorporation into the boney matrix. Moreover, a significant dose-dependent effect was observed between hPSC treatment groups. Thus and in summary, immunohistochemistry for

species-specific antigens verified that not only do hPSC play a direct role in bone formation, but also that hPSC play a role in paracrine support of host osteoprogenitor cell recruitment and/or differentiation.

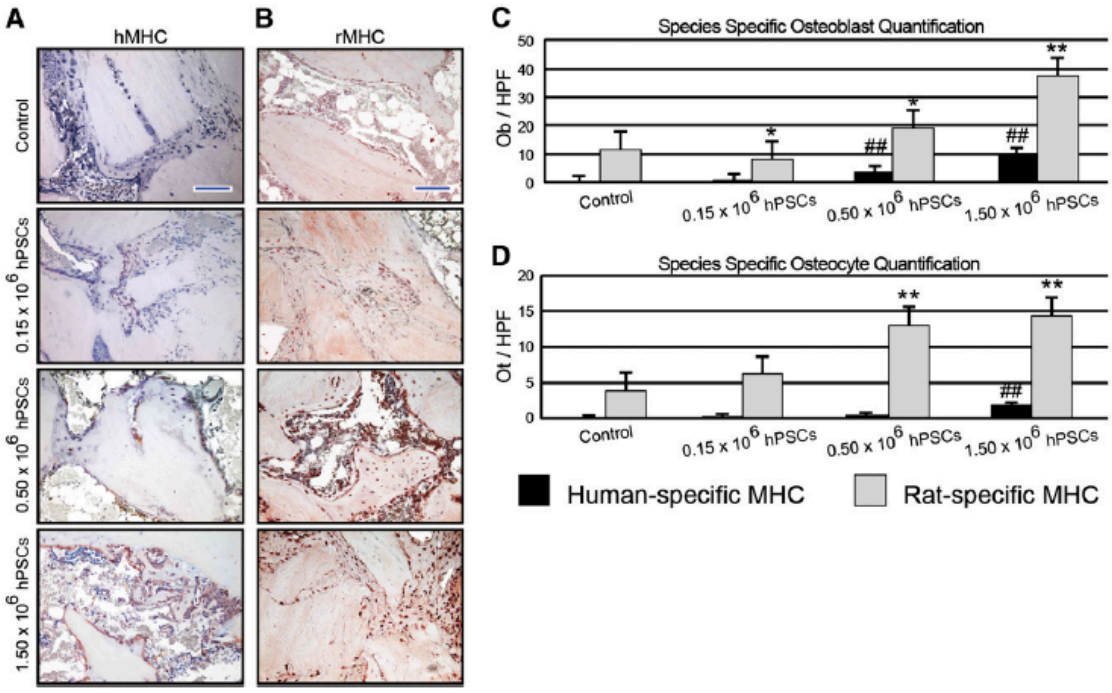

Figure 5. Species-Specific MHC Analyses. Immunohistochemical staining of (A) human- or (B) rat-specific Major Histocompatibility Complex (MHC). Quantifications for (C) Osteoblasts(Ob) and (D) Osteocytes(Ot) per higher power field (HPF); blue scale bar: 100μm; *$p \leq 0.05$ compared to rat-specific control values, **$p \leq 0.01$ compared to rat-specific control values; ##$p \leq 0.01$ compared to human-specific control values. A significant dose-dependent effect was observed between hPSC-treated groups.

Evaluation of the Matrix Deposition using Histomorphometric Analysis

Finally, *in vivo* fluorescent dye labeling images were analyzed to investigate new matrix deposition. Double calcein injections were performed (with a 7 day interval between injections), revealing increased calcein labeling among hPSC treated groups as well as clear double linear deposition in hPSC treated groups **(Fig. 10A)**. This was quantified, showing that hPSC treated samples exhibited a dose dependent increase in total calcein deposition **(Fig. 10B)**.

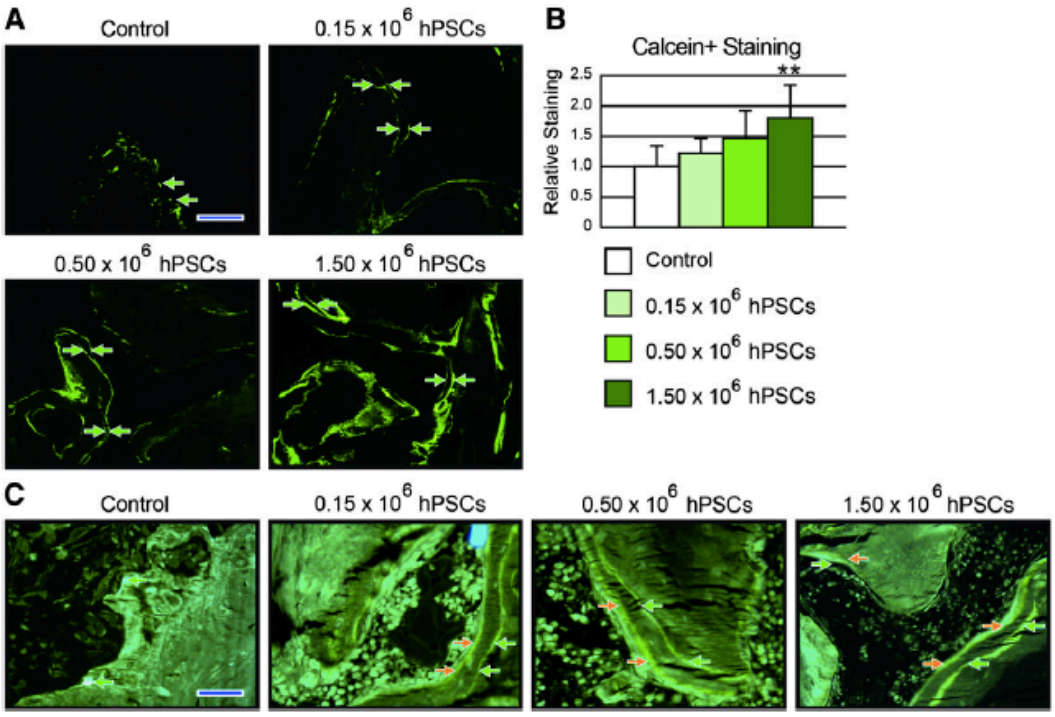

Figure 6. Bone Labeling Analyses. (A) Representative fluorescent microscopy pictures of Calcein/Calcein-labeled mineralization fronts of each treatment group. (B) Quantification of relative fluorescence of calcein/calcein mineralization fronts. (C) Representative fluorescent microscopy pictures of Calcein/demeclocycline-labeled mineralization fronts. Calcein: green, Demeclocycline: orange. A significant dose-dependent effect was observed in calcein staining between hPSC-treated groups.

Next, two fluorescent dye labeling was performed, this time using calcein (green) and demeclocyline (orange), again with a time interval of 7 days. In hPSC treated samples, a wide band of new-formed bone was apparent between green and orange labels **(Fig. 6C,** see green and orange arrows**)**. Overall, hPSC samples not only demonstrated increased bone formation, but also increased active bone mineralization.

Discussion

My data demonstrate that adipose-derived FACS purified hPSC delivered on a demineralized bone matrix scaffold – an osteoinductive matrix – can successfully induce functional bone tissue formation and reliable rat lumbar spinal. Prior to this study, evaluation of bone regeneration of hPSC were limited to non-functional bone regeneration models, including ectopic bone formation in a muscle pouch implant model[32] and re-ossification of calvarial bone defects[34]. Ectopic bone formation models are limited to validating *in vivo* osteogenic potential, and calvarial bone defects simply assess ossification and do not assess the functional properties of newly formed bone[44,45]. In contrast, spinal fusion models provide a more clinically relevant assessment of the newly formed bone, including bone quantity and biomechanical strength.

Spinal fusion is one of the most common procedures performed to achieve stability in spinal disorders. As previously discussed, autogenous bone grafting, the gold standard of care for spinal fusion procedures is limited in its use due to limited donor availability, additional surgical trauma and donor site morbidity[8-10]. Moreover, previously published rat spinal fusion studies assessing autologous bone grafting, were observed to yield an inferior fusion rate when compared to hPSC treatment (0% fusion after 4 weeks and 11% fusion after 8 weeks with autologous bone grafting, compared to 80-100% fusion in 4 weeks with hPSC treatment)[46,47]. MSC derived from multiple sources such as bone marrow and adipose tissue have attracted large interest for replacement of

autogenous bone in spinal fusion procedures[48-52]. Bone marrow stem cells (BMSC), however, are limited in supply and it is estimated that only one BMSC can be isolated per 100,000 cells [53]. To circumvent the shortage of MSC, readily isolatable methods such as selective cell retention[54] and ex vivo cell culture methods have been developed[48-50]. Selective cell retention of osteoprogenitors are clinically available using Cellect Graft Preparation system (Dupuy, Raynham, MA), however no clinical reports of success have been published[55]. Although ex vivo cell cultured MSC show promise towards successful spinal fusion rates ranging from 33% - 100% in animal studies[48-50,56-58], extended processing time, additional cost, and risks of contamination are still limiting factors to its use. Similarly, although ASC have been extensively studied in spinal fusion models with success[51,59,60], they possesses similar traits as BMSC in their culture-dependency. Since PSC are obtained from lipoaspirates and processed using FACS, a faster and contamination free source of osteoprogenitor cells can be obtained in comparison to bone marrow derived MSC.

My data has partially elucidated the mechanisms underlying purified hPSC mediated bone regeneration. Several possibilities have been proposed to explain the bone forming effects of hPSC. One explanation is the direct differentiation of hPSC into osteoblasts. Chen *et al.* have reported that pericytes undergo osteogenic differentiation *in vitro*[63], which has been subsequently verified in hPSC [32,33]. In the present study, we observed that hPSC undergo direct differentiation into bone forming cells, via the detection of human antigen among both newly formed osteoblasts and osteocytes *in vivo*. Notably, however, the majority of osteoblasts and osteocytes were in fact of host rat origin.

This observation leads to the other likely possibility that hPSC may not solely differentiate into bone-forming cells, but also lead to bone growth through predominantly trophic effects. For example, hPSC may induce local chemotaxis and differentiation of osteoprogenitor cells, as well as neovascularization of the implant site, as documented in other MSC types[27,33,64-67]. Prior studies have shown that pericytes secrete significantly greater quantities of various growth factors in comparison to traditional MSC sources, including heparin growth factors, fibroblast growth factors (FGF), and vascular endothelial growth factor (VEGF) [68]. These pro-osteogenic, pro-vasculogenic growth factors have been observed in high quantities after *in vivo* implantation, in both intramuscular[33], and calvarial defect models[34]. In addition, previous studies have observed that growth factors such as FGF have contributed to chemotaxis of stem cells[69-71]. In summary, although the mechanism in which hPSC form bone is currently only partially understood, we have shown that the implanted hPSC do not constitute the majority of bone-lining forming cells. This phenomenon has been frequently observed by other investigators and in other models of MSC implantation[72,73]. Thus, PSC have pleotropic functions to promote osteogenesis through both direct and indirect mechanisms along with supporting bone growth through increased vascularization.

Several recent studies have also expanded on the evolving relationship of perivascular progenitor cells to the cellular origin of MSCs within a microvascular environment. Currently, there is now exists ample experimental proof that perivascular cells give rise in culture to mesenchymal stem cells[74], but the relevance of these

observations to a possible natural role of perivascular cells as progenitors/regenerative cells in vivo is far less clear. The use of reporter mice has, however, recently brought evidence that perivascular cells – in particular pericytes – can act in situ as progenitors of white adipocytes[75], satellite cells and muscle fibers[76], follicular dendritic cells[77], and multiple other mesodermal cells[78]. Pericytes are also involved in myofibroblast generation and fibrosis development in the kidney, heart and skeletal muscle [79]. Better understanding the functions of their native perivascular predecessors will allow to further expand MSC application in tissue repair and wound healing.

Finally, my study has a number of limitations, which cautions extrapolation of my findings. For example, we evaluated three different dosages of hPSC application, and found slight variation in dose dependency of cell seeding density. Markers of bone matrix deposition showed a slight dose dependent increase between hPSC treatment groups, either by radiographic or histomorphometric analyses. In contrast, markers of osteoblastic differentiation showed a significant dose dependent effect between hPSC treatment groups. Specifically, a strong dose dependent effect was observed on rat osteoblast number, as well as species non-specific markers. Thus, we can hypothesize that should a longer period of study be undertaken, a dose-dependent effect in bone matrix deposition and/or spinal fusion may be observed. Another limitation of my study was sample size (n=5-6). Preliminary data yielded an anticipatory effect size of 2.0, suggesting n=5 would be sufficient for this study, however this was observed to be slightly conservative. Thus, future studies will be aimed to utilize a larger sample size and a longer study period in order to further investigate the dose-dependent effect of hPSC treatment.

Future studies must also be mindful of several intricacies in study design. Although the data presented herein possesses great promise, the current scientific standard for small animal spinal fusion assessment employ healthy and young animals. Unfortunately, this model does not appropriately reflect the challenging clinical conditions of older populations requiring spinal fusion, whom often possess an osteopenic/osteoporotic phenotype. As such, the utilization of ovariectomized or senile rodents may be required to test the true efficacy of experimental therapeutics. Additionally, to validate the findings presented herein, large animal studies will be necessary. Previous studies by Cui *et al.* and Shamsul *et al.* demonstrated the need to increase the number of MSC administered when translating from small to large animal studies. For instance, when $2x10^6$ BMSC were implanted in rats 100% fusion was observed[50], however, to induce spinal fusion in sheep, hydroxyapatite seeded in $5\text{-}6x10^7$ BMSC was required[80]. This drastic increase in the number of cells required is directly related to increasing phylogenic complexity and as such will complicate clinical translation. Thus, future studies should seek to incorporate growth factors to increase osteogenic potency, reduce the number of PSC or MSC required, and ultimately optimize successful fusion for large animal studies and human application.

References

1. Yelin E, Callahan LF. The economic cost and social and psychological impact of musculoskeletal conditions. National Arthritis Data Work Groups. Arthritis Rheum. 1995;38:1351-1362.

2. Aaos (2008) Burden of Musculoskeletal Diseases in the United States: Prevalence, Societal and Economic Cost: American Academy of Orthopaedic Surgeons.

3. Deyo RA, Gray DT, Kreuter W, et al. United States trends in lumbar fusion surgery for degenerative conditions. Spine (Phila Pa 1976). 2005;30:1441-1445; discussion 1446-1447.

4. Gray DT, Deyo RA, Kreuter W, et al. Population-based trends in volumes and rates of ambulatory lumbar spine surgery. Spine (Phila Pa 1976). 2006;31:1957-1963; discussion 1964.

5. Katz JN. Lumbar spinal fusion. Surgical rates, costs, and complications. Spine (Phila Pa 1976). 1995;20:78S-83S.

6. Lee CK, Langrana NA. A review of spinal fusion for degenerative disc disease: need for alternative treatment approach of disc arthroplasty? Spine J. 2004;4:173S-176S.

7. Taylor VM, Deyo RA, Cherkin DC, et al. Low back pain hospitalization. Recent United States trends and regional variations. Spine (Phila Pa 1976). 1994;19:1207-1212; discussion 1213.

8. Mikhael MM, Huddleston PM, Nassr A. Postoperative culture positive surgical site infections after the use of irradiated allograft, nonirradiated allograft, or autograft for spinal fusion. Spine (Phila Pa 1976). 2009;34:2466-2468.

9. Sawin PD, Traynelis VC, Menezes AH. A comparative analysis of fusion rates and donor-site morbidity for autogeneic rib and iliac crest bone grafts in posterior cervical fusions. J Neurosurg. 1998;88:255-265.

10. Wolfe SA. Complications of harvesting cranial bone grafts. Plast Reconstr Surg. 1996;98:567.

11. Deans RJ, Moseley AB. Mesenchymal stem cells: biology and potential clinical uses. Exp Hematol. 2000;28:875-884.

12. Minguell JJ, Conget P, Erices A. Biology and clinical utilization of mesenchymal progenitor cells. Braz J Med Biol Res. 2000;33:881-887.

13. Schwartz RE, Reyes M, Koodie L, et al. Multipotent adult progenitor cells from bone marrow differentiate into functional hepatocyte-like cells. J Clin Invest. 2002;109:1291-1302.

14. Moerman EJ, Teng K, Lipschitz DA, et al. Aging activates adipogenic and suppresses osteogenic programs in mesenchymal marrow stroma/stem cells: the role of PPAR-gamma2 transcription factor and TGF-beta/BMP signaling pathways. Aging Cell. 2004;3:379-389.

15. Giannoudis P, Tzioupis C, Almalki T, et al. Fracture healing in osteoporotic fractures: is it really different? A basic science perspective. Injury. 2007;38 Suppl 1:S90-99.

16. McIntosh K, Zvonic S, Garrett S, et al. The immunogenicity of human adipose-derived cells: temporal changes in vitro. Stem Cells. 2006;24:1246-1253.

17. Meliga E, Strem BM, Duckers HJ, et al. Adipose-derived cells. Cell Transplant. 2007;16:963-970.

18. De Ugarte DA, Morizono K, Elbarbary A, et al. Comparison of multi-lineage cells

from human adipose tissue and bone marrow. Cells Tissues Organs. 2003;174:101-109.

19. Aust L, Devlin B, Foster SJ, et al. Yield of human adipose-derived adult stem cells from liposuction aspirates. Cytotherapy. 2004;6:7-14.

20. Dahl JA, Duggal S, Coulston N, et al. Genetic and epigenetic instability of human bone marrow mesenchymal stem cells expanded in autologous serum or fetal bovine serum. Int J Dev Biol. 2008;52:1033-1042.

21. Niemeyer P, Kornacker M, Mehlhorn A, et al. Comparison of immunological properties of bone marrow stromal cells and adipose tissue-derived stem cells before and after osteogenic differentiation in vitro. Tissue Eng. 2007;13:111-121.

22. Paredes B, Santana A, Arribas MI, et al. Phenotypic differences during the osteogenic differentiation of single cell-derived clones isolated from human lipoaspirates. J Tissue Eng Regen Med. 2011;5:589-599.

23. Rajashekhar G, Traktuev DO, Roell WC, et al. IFATS collection: Adipose stromal cell differentiation is reduced by endothelial cell contact and paracrine communication: role of canonical Wnt signaling. Stem Cells. 2008;26:2674-2681.

24. Meury T, Verrier S, Alini M. Human endothelial cells inhibit BMSC differentiation into mature osteoblasts in vitro by interfering with osterix expression. J Cell Biochem. 2006;98:992-1006.

25. Crisan M, Yap S, Casteilla L, et al. A perivascular origin for mesenchymal stem cells in multiple human organs. Cell Stem Cell. 2008;3:301-313.

26. Crisan M, Chen CW, Corselli M, et al. Perivascular multipotent progenitor cells in human organs. Ann N Y Acad Sci. 2009;1176:118-123.

27. Crisan M, Corselli M, Chen CW, et al. Multilineage stem cells in the adult: a perivascular legacy? Organogenesis. 2011;7:101-104.

28. Crisan M, Deasy B, Gavina M, et al. Purification and long-term culture of multipotent progenitor cells affiliated with the walls of human blood vessels: myoendothelial cells and pericytes. Methods Cell Biol. 2008;86:295-309.

29. Corselli M, Chen CW, Crisan M, et al. Perivascular ancestors of adult multipotent stem cells. Arterioscler Thromb Vasc Biol. 2010;30:1104-1109.

30. Corselli M, Chen CW, Sun B, et al. The tunica adventitia of human arteries and veins as a source of mesenchymal stem cells. Stem Cells Dev. 2012;21:1299-1308.

31. Zhang X, Peault B, Chen W, et al. The Nell-1 growth factor stimulates bone formation by purified human perivascular cells. Tissue Eng Part A. 2011;17:2497-2509.

32. James A, Zara J. , et al. (2012) Perivascular Stem Cells: A Prospectively Purified Mesenchymal Stem Cell Population for Bone Tissue Engineering. Stem Cells Translational Medicine pp. 510-519.

33. Askarinam A, James AW, Zara JN, et al. Human Perivascular Stem Cells Show Enhanced Osteogenesis and Vasculogenesis with NELL-1 Protein. Tissue Eng Part A. 2013.

34. James A, Zara J. , et al. (2012) An Abundant Perivascular Source of Stem Cells for Bone Tissue Engineering.

35. Li W, Lee M, Whang J, et al. Delivery of lyophilized Nell-1 in a rat spinal fusion model. Tissue Eng Part A. 2010;16:2861-2870.

36. Grauer JN, Patel TC, Erulkar JS, et al. 2000 Young Investigator Research Award

winner. Evaluation of OP-1 as a graft substitute for intertransverse process lumbar fusion. Spine (Phila Pa 1976). 2001;26:127-133.

37. Parfitt AM, Drezner MK, Glorieux FH, et al. Bone histomorphometry: standardization of nomenclature, symbols, and units. Report of the ASBMR Histomorphometry Nomenclature Committee. J Bone Miner Res. 1987;2:595-610.

38. Odgaard A, Linde F. The underestimation of Young's modulus in compressive testing of cancellous bone specimens. J Biomech. 1991;24:691-698.

39. Keaveny TM, Pinilla TP, Crawford RP, et al. Systematic and random errors in compression testing of trabecular bone. J Orthop Res. 1997;15:101-110.

40. Zhu M, Keller TS, Spengler DM. Effects of specimen load-bearing and free surface layers on the compressive mechanical properties of cellular materials. J Biomech. 1994;27:57-66.

41. Lu SS, Zhang X, Soo C, et al. The osteoinductive properties of Nell-1 in a rat spinal fusion model. Spine J. 2007;7:50-60.

42. Kuo CS, Hu HT, Lin RM, et al. Biomechanical analysis of the lumbar spine on facet joint force and intradiscal pressure--a finite element study. BMC Musculoskelet Disord. 2010;11:151.

43. Lee M, Li W, Siu RK, et al. Biomimetic apatite-coated alginate/chitosan microparticles as osteogenic protein carriers. Biomaterials. 2009;30:6094-6101.

44. Scott MA, Levi B, Askarinam A, et al. Brief review of models of ectopic bone formation. Stem Cells Dev. 2012;21:655-667.

45. Spicer PP, Kretlow JD, Young S, et al. Evaluation of bone regeneration using the rat

critical size calvarial defect. Nat Protoc. 2012;7:1918-1929.

46. Koerner JD, Yalamanchili P, Munoz W, et al. The effects of local insulin application to lumbar spinal fusions in a rat model. Spine J. 2013;13:22-31.

47. Yuan W, James AW, Asatrian G, et al. NELL-1 based demineralized bone graft promotes rat spine fusion as compared to commercially available BMP-2 product. J Orthop Sci. 2013;18:646-657.

48. Gupta MC, Theerajunyaporn T, Maitra S, et al. Efficacy of mesenchymal stem cell enriched grafts in an ovine posterolateral lumbar spine model. Spine (Phila Pa 1976). 2007;32:720-726; discussion 727.

49. Minamide A, Yoshida M, Kawakami M, et al. The use of cultured bone marrow cells in type I collagen gel and porous hydroxyapatite for posterolateral lumbar spine fusion. Spine (Phila Pa 1976). 2005;30:1134-1138.

50. Cui Q, Ming Xiao Z, Balian G, et al. Comparison of lumbar spine fusion using mixed and cloned marrow cells. Spine (Phila Pa 1976). 2001;26:2305-2310.

51. Lopez MJ, McIntosh KR, Spencer ND, et al. Acceleration of spinal fusion using syngeneic and allogeneic adult adipose derived stem cells in a rat model. J Orthop Res. 2009;27:366-373.

52. Miyazaki M, Zuk PA, Zou J, et al. Comparison of human mesenchymal stem cells derived from adipose tissue and bone marrow for ex vivo gene therapy in rat spinal fusion model. Spine (Phila Pa 1976). 2008;33:863-869.

53. Bruder SP, Jaiswal N, Ricalton NS, et al. Mesenchymal stem cells in osteobiology and applied bone regeneration. Clin Orthop Relat Res. 1998;S247-256.

54. Muschler GF, Matsukura Y, Nitto H, et al. Selective retention of bone

marrow-derived cells to enhance spinal fusion. Clin Orthop Relat Res. 2005;242-251.

55. McLain RF, Fleming JE, Boehm CA, et al. Aspiration of osteoprogenitor cells for augmenting spinal fusion: comparison of progenitor cell concentrations from the vertebral body and iliac crest. J Bone Joint Surg Am. 2005;87:2655-2661.

56. Wang T, Dang G, Guo Z, et al. Evaluation of autologous bone marrow mesenchymal stem cell-calcium phosphate ceramic composite for lumbar fusion in rhesus monkey interbody fusion model. Tissue Eng. 2005;11:1159-1167.

57. Kai T, Shao-qing G, Geng-ting D. In vivo evaluation of bone marrow stromal-derived osteoblasts-porous calcium phosphate ceramic composites as bone graft substitute for lumbar intervertebral spinal fusion. Spine (Phila Pa 1976). 2003;28:1653-1658.

58. Nakajima T, Iizuka H, Tsutsumi S, et al. Evaluation of posterolateral spinal fusion using mesenchymal stem cells: differences with or without osteogenic differentiation. Spine (Phila Pa 1976). 2007;32:2432-2436.

59. Zeng Q, Li X, Beck G, et al. Growth and differentiation factor-5 (GDF-5) stimulates osteogenic differentiation and increases vascular endothelial growth factor (VEGF) levels in fat-derived stromal cells in vitro. Bone. 2007;40:374-381.

60. Hsu WK, Wang JC, Liu NQ, et al. Stem cells from human fat as cellular delivery vehicles in an athymic rat posterolateral spine fusion model. J Bone Joint Surg Am. 2008;90:1043-1052.

61. Kwon B, Jenis LG. Carrier materials for spinal fusion. Spine J. 2005;5:224S-230S.

62. Park JJ, Hershman SH, Kim YH. Updates in the use of bone grafts in the lumbar

spine. Bull Hosp Jt Dis (2013). 2013;71:39-48.

63. Chen CW, Corselli M, Peault B, et al. Human blood-vessel-derived stem cells for tissue repair and regeneration. J Biomed Biotechnol. 2012;2012:597439.

64. Feng J, Mantesso A, Sharpe PT. Perivascular cells as mesenchymal stem cells. Expert Opin Biol Ther. 2010;10:1441-1451.

65. James AW, Zara JN, Corselli M, et al. Use of human perivascular stem cells for bone regeneration. J Vis Exp. 2012.

66. Tottey S, Corselli M, Jeffries EM, et al. Extracellular matrix degradation products and low-oxygen conditions enhance the regenerative potential of perivascular stem cells. Tissue Eng Part A. 2011;17:37-44.

67. Udani VM, Santarelli JG, Yung YC, et al. Hematopoietic stem cells give rise to perivascular endothelial-like cells during brain tumor angiogenesis. Stem Cells Dev. 2005;14:478-486.

68. Chen CW, Montelatici E, Crisan M, et al. Perivascular multi-lineage progenitor cells in human organs: regenerative units, cytokine sources or both? Cytokine Growth Factor Rev. 2009;20:429-434.

69. Ozaki Y, Nishimura M, Sekiya K, et al. Comprehensive analysis of chemotactic factors for bone marrow mesenchymal stem cells. Stem Cells Dev. 2007;16:119-129.

70. Uchida K, Urabe K, Naruse K, et al. Comparison of the cytokine-induced migratory response between primary and subcultured populations of rat mesenchymal bone marrow cells. J Orthop Sci. 2007;12:484-492.

71. Ponte AL, Marais E, Gallay N, et al. The in vitro migration capacity of human bone

marrow mesenchymal stem cells: comparison of chemokine and growth factor chemotactic activities. Stem Cells. 2007;25:1737-1745.

72. Oshima Y, Watanabe N, Matsuda K, et al. Behavior of transplanted bone marrow-derived GFP mesenchymal cells in osteochondral defect as a simulation of autologous transplantation. J Histochem Cytochem. 2005;53:207-216.

73. Oshima Y, Watanabe N, Matsuda K, et al. Fate of transplanted bone-marrow-derived mesenchymal cells during osteochondral repair using transgenic rats to simulate autologous transplantation. Osteoarthritis Cartilage. 2004;12:811-817.

74. Murray IR, West CC, Hardy WR, et al. Natural history of mesenchymal stem cells, from vessel walls to culture vessels. Cell Mol Life Sci. 2014;71:1353-1374.

75. Tang W, Zeve D, Suh JM, et al. White fat progenitor cells reside in the adipose vasculature. Science. 2008;322:583-586.

76. Dellavalle A, Maroli G, Covarello D, et al. Pericytes resident in postnatal skeletal muscle differentiate into muscle fibres and generate satellite cells. Nat Commun. 2011;2:499.

77. Krautler NJ, Kana V, Kranich J, et al. Follicular dendritic cells emerge from ubiquitous perivascular precursors. Cell. 2012;150:194-206.

78. Olson LE, Soriano P. PDGFRbeta signaling regulates mural cell plasticity and inhibits fat development. Dev Cell. 2011;20:815-826.

79. Henderson NC, Arnold TD, Katamura Y, et al. Targeting of alphav integrin identifies a core molecular pathway that regulates fibrosis in several organs. Nat Med. 2013;19:1617-1624.

80. Shamsul BS, Tan KK, Chen HC, et al. Posterolateral spinal fusion with ostegenesis

induced BMSC seeded TCP/HA in a sheep model. Tissue Cell. 2014;46:152-158.

81. Oedayrajsingh-Varma MJ, van Ham SM, Knippenberg M, et al. Adipose tissue-derived mesenchymal stem cell yield and growth characteristics are affected by the tissue-harvesting procedure. Cytotherapy. 2006;8:166-177.

82. Jurgens WJ, Oedayrajsingh-Varma MJ, Helder MN, et al. Effect of tissue-harvesting site on yield of stem cells derived from adipose tissue: implications for cell-based therapies. Cell Tissue Res. 2008;332:415-426.